# Ocean biogeochemical response to phytoplankton-light feedback in a global model

Manfredi Manizza,[1,2,3] Corinne Le Quéré,[2,4] Andrew J. Watson,[2] and Erik T. Buitenhuis[2]

Received 7 August 2007; revised 27 February 2008; accepted 5 June 2008; published 14 October 2008.

[1] Oceanic phytoplankton, absorbing solar radiation, can influence the bio-optical properties of seawater and hence upper ocean physics. We include this process in a global ocean general circulation model (OGCM) coupled to a dynamic green ocean model (DGOM) based on multiple plankton functional types (PFT). We not only study the impact of this process on ocean physics but we also explore the biogeochemical response due to this biophysical feedback. The phytoplankton-light feedback (PLF) impacts the dynamics of the upper tropical and subtropical oceans. The change in circulation enhances both the vertical supply in the tropics and the lateral supply of nutrients from the tropics to the subtropics boosting the subtropical productivity by up to 60 gC $m^{-2}$ $a^{-1}$. Physical changes, due to the PLF, impact on light and nutrient availability causing shifts in the ocean ecosystems. In the extratropics, increased stratification favors calcifiers (by up to $\sim$8%) at the expense of mixed phytoplankton. In the Southern Ocean, silicifiers increase their biomass (by up to $\sim$10%) because of the combined alleviation of iron and light limitation. The PLF has a small effect globally on air-sea fluxes of carbon dioxide ($CO_2$, 72 TmolC $a^{-1}$ outgassing) and oxygen ($O_2$, 46 Tmol$O_2$ $a^{-1}$ ingassing) because changes in biogeochemical processes (primary production, biogenic calcification, and export production) highly vary regionally and can also oppose each other. From our study it emerges that the main impact of the PLF is an amplification of the seasonal cycle of physical and biogeochemical properties of the high-latitude oceans mostly driven by the amplification of the SST seasonal cycle.

**Citation:** Manizza, M., C. Le Quéré, A. J. Watson, and E. T. Buitenhuis (2008), Ocean biogeochemical response to phytoplankton-light feedback in a global model, *J. Geophys. Res.*, *113*, C10010, doi:10.1029/2007JC004478.

## 1. Introduction

[2] Marine phytoplankton absorb solar radiation to carry out photosynthesis in the surface ocean. Because they absorb solar radiation they modify the vertical distribution of light and thus heat throughout the water column, impacting the physical properties of the upper ocean such as temperature, stratification and sea ice. Using satellite data [*Kahru et al.*, 1993] estimated that localized blooms of cyanobacteria increased sea surface temperature (SST) by up to 1.5°C because of their heat absorption.

[3] Several authors have studied how marine phytoplankton can impact the physical properties of the upper ocean using a wide range of ocean models which range from simple mixed layer models [*Sathyendranath et al.*, 1991] to OGCMs [*Nakamoto et al.*, 2000, 2001; *Murtugudde et al.*, 2002], and simplified climate models [*Timmermann and Jin*, 2002; *Marzeion et al.*, 2005]. These modeling studies particularly focused on the tropical oceans.

[4] Recently, other studies have attempted to quantify the effect of PLF on ocean climate on a global scale [*Shell et al.*, 2003; *Kara et al.*, 2004; *Manizza et al.*, 2005; *Sweeney et al.*, 2005; *Wetzel et al.*, 2006]. Most of the published studies used satellite data only (CZCS and SeaWiFS) to represent the spatial and temporal distribution of chlorophyll concentration. Only a few studies [*Oschlies*, 2004; *Manizza et al.*, 2005; *Wetzel et al.*, 2006] have attempted to explore the full biophysical feedbacks using coupled physical-biological ocean models. In our previous study [*Manizza et al.*, 2005] we have shown that in the extratropical zones, the PLF amplifies the seasonal cycle of SST by up to 1.2° and of the mixed layer depth (MLD) by up to $\sim$30 m (zonal average). The amplification of the SST seasonal cycle also results in an amplification of the seasonal cycle of sea-ice cover (SIC) by up $\sim$8%. The mechanism inducing this amplification has been also elucidated in some previous studies [*Shell et al.*, 2003; *Manizza et al.*, 2005]. For instance, *Manizza et al.* [2005] showed that this biophysical feedback can also affect SIC, because of the higher phytoplankton growth during the polar summers due to faster sea-ice melting and greater light availability. The impact of this PLF to SIC has also been shown by *Wetzel et al.* [2006] in a

[1]Max-Planck-Institut für Biogeochemie, Jena, Germany.
[2]School of Environmental Sciences, University of East Anglia, Norwich, UK.
[3]Now at Program in Atmospheres, Oceans, and Climate, Department of Earth, Atmospheric and Planetary Sciences, Massachusetts Institute of Technology, Cambridge, Massachusetts, USA.
[4]British Antarctic Survey, Cambridge, UK.


0148-0227/08/2007JC004478$09.00

**Table 1.** List of Key Physiological Parameters Particular to Each Phytoplankton Function Group Represented in the Version of PlankTOM5 Used for This Study[a]

| PFT | $K_P$ ($\mu$M) | $K_{Fe}$ (nM) | $K_{Si}$ ($\mu$M) |
|---|---|---|---|
| Mixed phytoplankton | 0.13 | 0.25 | |
| Calcifiers | 0.03 | 0.25 | |
| Silicifiers | 0.53 | 0.12 | 4.0 |

[a] $K_P$, $K_{Fe}$, and $K_{Si}$ are half-saturation constants of phytoplankton growth for phosphorus, iron, and silica, respectively.

global coupled climate model. A modeling study by *Oschlies* [2004] has shown that the PLF can also impact the biogeochemical processes such as primary production in the North Atlantic Ocean.

[5] In this study we follow the same methodological approach used by *Oschlies* [2004] but we add three new features. (1) We extend the geographical scope from regional to global scale. (2) We use a more complex DGOM based on ecosystem dynamics of multiple PFT rather than a simple NPZD ecosystem model as used by *Oschlies* [2004]. (3) We also quantify the impact of the PLF on the air-sea fluxes of $CO_2$ and $O_2$.

[6] We use an Ocean Biogeochemical General Circulation Model (OBGCM) which computes both the physical and the biogeochemical properties of the global ocean. The OBGCM allows us to understand how the presence of phytoplankton biomass perturbs the physical environment and what are the consequences of these perturbations for the biogeochemical processes.

[7] This paper is organized as follows: In section 2, we describe the components of the OBGCM and the modeling strategy adopted for this study. In section 3, we report and comment on the changes in both the physical and the biogeochemical processes, and their impact on air-sea fluxes of $CO_2$ and $O_2$. In section 4 we conclude by commenting on the role of this biophysical feedback and its potential interaction with a future changing climate.

## 2. OBGCM Description

### 2.1. Physical Sea-Ice-Ocean Component

[8] We use the ORCA-LIM model, an OGCM that includes sea ice [*Timmermann et al.*, 2005] to explicitly represent the physical processes of the global ocean. The ocean physical component of ORCA-LIM is OPA, an OGCM based on primitive equations [*Madec et al.*, 1999]. OPA implements a global irregular mesh with variable resolution [*Madec and Imbard*, 1996]. The longitudinal resolution is 2° everywhere, whereas latitudinal horizontal resolution varies form 2° at mid latitudes (between ~15° and ~25°) to 0.5° at the equator and at the poles. OPA has 31 vertical levels with vertical resolution of 10 m in the top 100 m. OPA also includes a 1.5-order turbulent kinetic energy model [*Gaspar et al.*, 1990] that computes vertical mixing throughout the water column. OPA implicitly represents the eddy-induced mixing processes with the [*Gent and McWilliams*, 1990] parameterization.

[9] The sea ice component of ORCA-LIM is the Louvain-la-Neuve Sea Ice Model (LIM) [*Fichefet and Morales-Maqueda*, 1999], a dynamic-thermodynamic model specific for climate studies. LIM is composed of three layers (one for the snow and two for the sea ice). It computes sea-ice thickness, extension, and motion.

### 2.2. Ocean Biogeochemistry Component

[10] We couple ORCA-LIM to the PlankTOM5 model, a state-of-the-art DGOM model, the same version used in our previous study [*Manizza et al.*, 2005]. PlankTOM5 is based on the explicit representation of ecosystem dynamics of multiple PFT [*Le Quéré et al.*, 2005]. It builds on the PISCES model [*Aumont et al.*, 2003] already used in some previous studies of the ocean carbon cycle for different climatic scenarios [*Bopp*, 2001; *Bopp et al.*, 2003].

[11] PlankTOM5 represents five PFT, three phytoplankton (mixed phytoplankton, silicifiers and calcifiers) and two zooplankton (micro and meso) functional types. Growth of phytoplankton functional types is colimited by light, phosphorus, silica and iron with PFT specific affinities (Table 1).

[12] The export of particulate organic carbon (POC) is driven by the sinking of two classes of particles (small and big POC) that have different sinking rates, 3 and 50 m $d^{-1}$, respectively. Small POC particles are fed by mixed phytoplankton, calcifiers, and microzooplankton whereas big POC particles are fed by silicifiers and mesozooplankton. Pelagic biogenic calcification is carried out by calcifiers. Calcium carbonate ($CaCO_3$) sinks at the same speed as big POC particles.

[13] The evolution of each prognostic variable J in the model is governed by the processes of advection (first term in equation (1)), diffusion (second term in equation (1)) and all the biogeochemical processes generically expressed as SMS (Source Minus Sink, third term in equation (1)), as follows:

$$\frac{dJ}{dt} = u\nabla J + \nabla(K\nabla J) + SMS, \quad (1)$$

where $K$ represents both the lateral and vertical tracer diffusion coefficients and $u$ is velocity. PlankTOM5 is coupled online to ORCA-LIM which computes the dynamical fields used for the advection of the biogeochemical tracers. PlankTOM5 also has full ocean carbon and oxygen cycles. The air-sea fluxes are computed, both for $CO_2$ and $O_2$, according to *Wanninkhof* [1992] applying the following formulation:

$$Flux_{(air-sea)} = (1-\gamma)\cdot\alpha\cdot k_v\cdot\Delta C, \quad (2)$$

where $\gamma$ is the sea ice cover fraction, $\alpha$ is the solubility of the gas in seawater [*Weiss*, 1970]. Here $k_v$ is the gas transfer velocity (or "piston velocity") which increases with wind speed owing to an increased roughness of the ocean surface. $\Delta C$ is the air-sea difference of partial pressure of the gas (both $CO_2$ and $O_2$). For $CO_2$ we correct the partial pressure to 100% humidity following *Sarmiento et al.* [1992].

### 2.3. Bio-optical Modeling

[14] To isolate the effect of the PLF, we run the same OBGCM but using two different parameterizations for the penetration of light throughout the water column as in work by *Manizza et al.* [2005].

[15] We label as Blue Ocean the version of the OBGCM where the penetration of solar radiation in the water column depends on the physical properties of seawater for the mean open ocean conditions. The value of irradiance at every vertical level of the ocean model is computed by splitting the total surface irradiance $I_o$ in two wavelength bands [*Paulson and Simpson*, 1977],

$$I_{(z)} = I_{IR} \cdot e^{-k_{IR}z} + I_{VIS} \cdot e^{-k_{VIS}z}, \quad (3)$$

where the first and second right-hand terms represent the penetration of infrared and visible wavelength bands, respectively. The light attenuation coefficients $k_{IR}$ = 2.86 $m^{-1}$ (corresponding to a penetration depth of 0.35 m) and $k_{VIS}$ = 0.0434 $m^{-1}$ (corresponding to a penetration depth of 23 m) and the light partitioning ($I_{IR} = I_0 \cdot (0.58)$ and $I_{VIS} = I_0 \cdot (0.42)$) were estimated for mean open ocean conditions. z is depth. In the Blue Ocean simulation the light attenuation coefficients both for the infrared and for the visible part of the light are constant in time and space.

[16] In the second version of the OBGCM labeled Green Ocean, we consider the influence of spatial and temporal variability of [Chl] on the vertical penetration of the light as follows:

$$I_{(z)} = I_{IR} \cdot e^{-k_{IR}z} + I_{RED(z-1)} \cdot e^{-k_{(r)}\Delta z} + I_{BLUE(z-1)} \cdot e^{-k_{(b)}\Delta z}, \quad (4)$$

where $\Delta$z is the thickness of each layer between two vertical levels.

[17] We compute the light attenuation coefficient ($k$), for the two bands as a function of chlorophyll concentration ([Chl] in mg $m^{-3}$) [*Morel*, 1988],

$$k_{(\lambda)} = k_{sw(\lambda)} + \chi_{(\lambda)} \cdot [Chl]^{e_{(\lambda)}}. \quad (5)$$

The coefficients are derived from the visible light spectrum [*Morel*, 1988] and are averaged in two bands [*Ballé*, 1998; *Foujols et al.*, 2000]. Here $\lambda$ is either red (r) or blue/green (b), $k_{sw(\lambda)}$ is the light attenuation coefficient for optically pure seawater with values of 0.225 and 0.0232 $m^{-1}$ for red and blue/green respectively, $\chi_{(\lambda)}$ is 0.037 and 0.074 $m^{-2}$ $mgChl^{-1}$ for the red and blue/green band, respectively, and $e_{(\lambda)}$ is 0.629 for red and 0.674 for the blue/green (no units).

[18] The [Chl] used to derive the light attenuation coefficient is the sum of the [Chl] of mixed phytoplankton, calcifiers and silicifiers. The two-band parameterization used to represent the visible light penetration is used in both versions of the OBGCM to calculate the irradiance at depth for the computation of primary production [*Foujols et al.*, 2000].

### 2.4. OBGCM Forcing and Experiment Setup

[19] We force the OBGCM with the NCEP reanalyzed daily forcing [*Kalnay et al.*, 1996]. We use fresh water fluxes, shortwave solar radiation (used both for the thermal heating forcing and for the computation of photosynthesis), air temperature and wind stress. The heat fluxes are computed by the OBGCM using the imposed air temperature at 2 m and the computed SST using bulk formulas according to *Goosse* [1997].

[20] In both simulations we initialize the models with the following global observation fields (temperature, salinity, phosphate [$PO_4$] and silicate [$Si(OH)_4$] concentrations, respectively) from the World Ocean Atlas [*Levitus*, 1982; *Conkright et al.*, 2002]. Dissolved Inorganic Carbon (DIC) and Alkalinity fields are taken from are taken from the GLODAP climatology [*Key et al.*, 2004] and dissolved oxygen from *Levitus and Boyer* [1994]. For Detritus (big and small particles of organic carbon) and PFT distributions, we use restart files from previous runs. We run the model from 1990 to 2000 and report here results of the last year.

## 3. Results

[21] In this section we show the differences of the results between the two versions of the OBGCM (Green Ocean minus Blue Ocean) to isolate the effect of the PLF on physical and biogeochemical processes.

### 3.1. Global Impact on Irradiance

[22] The presence of phytoplankton biomass impacts the penetration of irradiance reducing the level of irradiance at depth. It is evident, as expected, that the reduction of irradiance at depth show the highest values in the most productive (high latitudes and Equatorial Pacific Ocean) areas of the global ocean and the least values in the least productive ares (subtropical gyres of both hemispheres). Relative to the levels of irradiance calculated in the Blue Ocean version of our OBGCM, in the high-latitude oceans the presence of phytoplankton biomass reduces the irradiance by up to 50% at 10 m and by up to 100% at 60 m (Figure 1). However in the subtropical gyres the reduction is by up to 20% at 10 m and is by up to 5% at 60 m (Figure 1). Furthermore, in order to better estimate the impact of the phytoplankton presence on light fields, we also calculated the difference of penetration depth of irradiance ($Z_p$) between the Green Ocean and Blue Ocean version of our OBGCM. We define the $Z_p$ as follows:

$$Z_p = \frac{\int_0^{-z} I_{(z)}\, dz}{I_0}, \quad (6)$$

where $I_{(z)}$ is irradiance at depth, $I_0$ is irradiance at surface, and $z$ is depth. In the Blue Ocean version of the model, the penetration depth of the visible is 23 m everywhere. The PLF reduces by up to ~7 (~30% reduction) in the highly productive areas such as high-latitude oceans of both hemispheres and the Equatorial Pacific (Figure 1, bottom) whereas it causes a smaller reduction (~13% reduction) in the low productive regions such as the subtropical gyres of both hemispheres.

### 3.2. Upper Ocean Physics and Dynamics

[23] The PLF has several consequences for the upper ocean physical structure. We can summarize the effects of the PLF in two main categories: First, the direct effects due the thermodynamical effect of heat trapping. Second, the indirect effect due to the change in ocean circulation.

[24] In the extratropical zones, the PLF has a direct impact on ocean physics: (1) it warms the surface layers where phytoplankton live and (2) it cools the subsurface

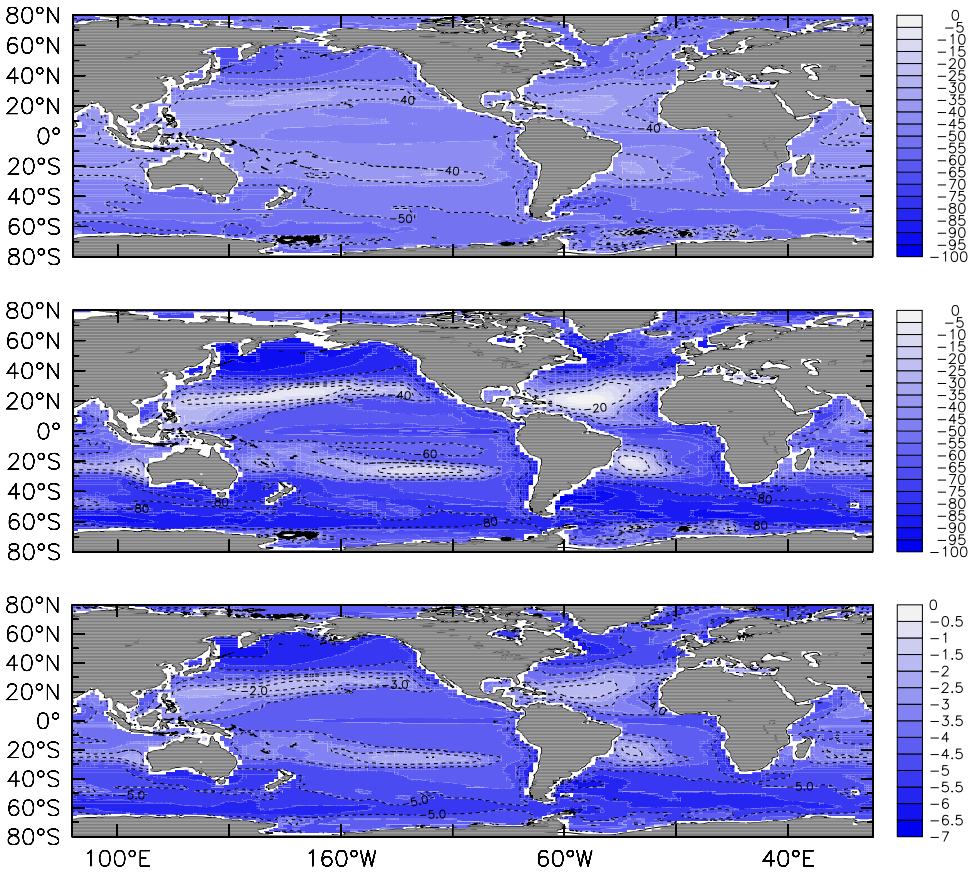


**Figure 1.** Annual average of difference of irradiance at (top) 10 meter and (middle) 60 m depth and of (bottom) $Z_p$. Units are (top and middle) percent and (bottom) meters.

layers underneath [*Manizza*, 2006]. The second process is a direct consequence of the first process because of the stronger heat trapping at the surface. Such mechanism produces an amplification the seasonal cycle of SST (Figure 2, top) and consequently of sea-ice cover (Figure 2, bottom). In our previous study we mostly focused on the impact of the PLF in the extratropical zones (north and south of 10° of each hemisphere). Here we highlight the impact on the tropical oceans.

[25] In the tropical zones the dominant effect is indirect. The PLF induces modifications of the local patterns of circulation producing an indirect physical effect that masks the direct effect. The PLF causes an increase in the surface currents flowing from the tropics to the subtropics. *Sweeney et al.* [2005] tested in an OGCM different bio-optical parameterizations and they suggested that the change in MLD has a direct impact on the velocity of water flowing from the tropics to the subtropics. They have shown that the efficiency of the horizontal pressure gradient ($\frac{\partial p}{\partial x}$) at driving meridional transport depends on the depth of integration limited by the MLD. This latter is impacted by the PLF which causes a general shoaling of the MLD as shown here (Figure 2, middle) and in our previous study [*Manizza et al.*, 2005]. Our results, as theirs, confirm that currents velocity (Figure 3) at surface from the tropics to the subtropics are sensitive to the change in the MLD in the tropics. This enhancement of meridional component of currents velocity also induces an increase in the currents velocity equatorward at the subsurface (∼50 m) to balance the enhancement of the poleward flow at the surface (Figure 3). The changes in ocean circulation at different depths must be balanced by an increase in upwelling at the equator that closes the dynamical balance of the subtropical cells and is the primary source of SST cooling in the tropics. Our results [*Manizza et al.*, 2005] also confirm the SST cooling effect in the tropics reported in other studies [*Nakamoto et al.*, 2001; *Shell et al.*, 2003] where bio-optical parameterizations similar to ours have been implemented. Furthermore, the shoaling of the MLD in the tropical Atlantic and Pacific Oceans produces an upward displacement of Equatorial UnderCurrent (EUC) (Figure 4, right) that impacts the nutrient supply with consequences for the primary production of the tropical Atlantic and Pacific Ocean (see section 3.5 for a more detailed discussion).

### 3.3. Surface Nutrient Distributions

[26] The modifications of the physical properties of the ocean have consequences for the surface distribution of nutrients.

[27] In the tropical Atlantic and Pacific oceans, the increase both in upwelling and in lateral advection toward midlatitudes at the surface causes an increase in surface phosphorus ([P]) by up to 0.2 $\mu$M (Figure 5, top left).

[28] The extra supply of [P] in the tropics is advected to the subtropical gyres with a large fertilizing effect on the

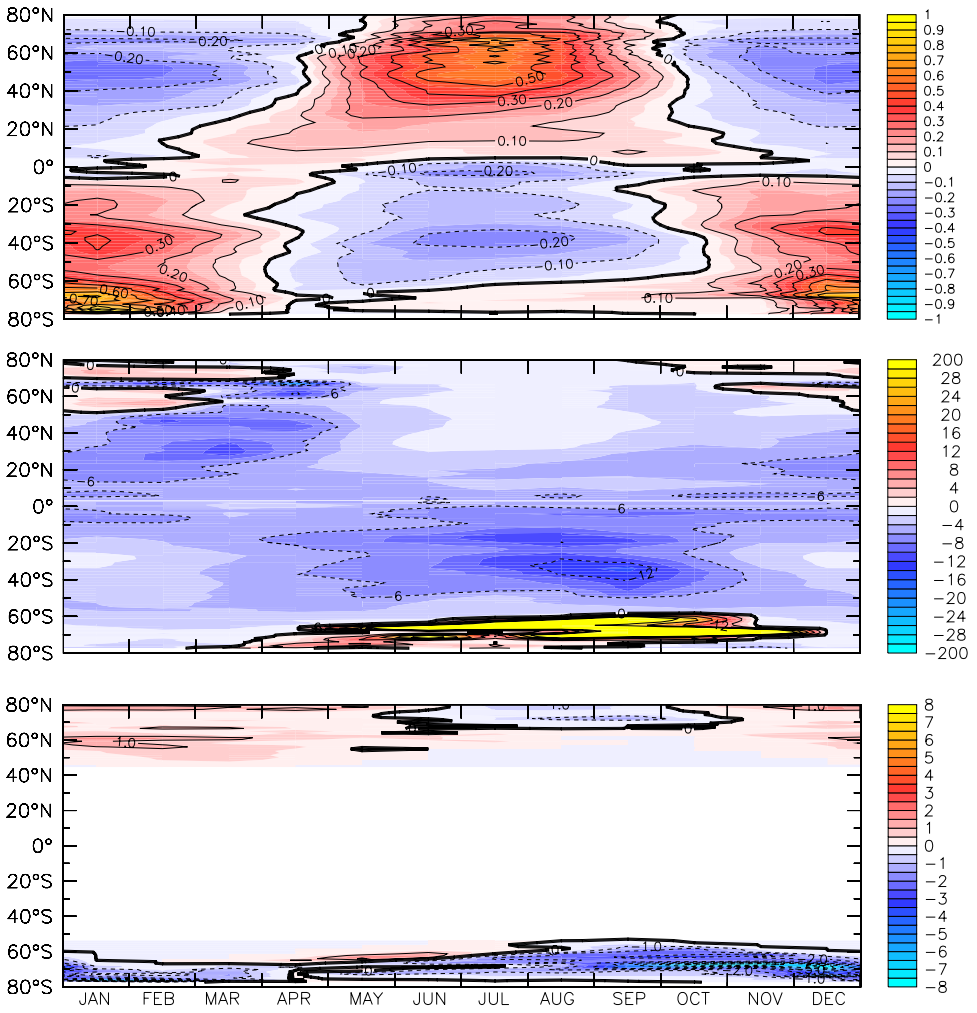


**Figure 2.** Time/latitude plot of difference (Green Ocean minus Blue Ocean) in (top) SST, (middle) MLD, and (bottom) SIC. Units are °C, meters, and percent, respectively.

productivity of those areas (see section 3.5 for a more detailed description).

[29] At high latitudes of both hemispheres, the biophysical feedback modifies the nutrient distribution at the ocean surface via two mechanisms acting differently in summer and winter. In spring/summer the PLF increases the stability of the water column (Figure 2, middle) and causes a more efficient uptake of nutrients, which then decrease in the top layers of the ocean. However, in fall/winter the PLF causes an increase in the vertical mixing (Figure 2, middle). This increase is due to the enhanced loss of buoyancy driven by the mixing of surface layers with colder subsurface layers [*Manizza*, 2006]. Moreover, in some localized areas a reduction of SIC (Figure 2, bottom) leads to an increase in the area of ocean available for atmospheric forcing and vertical mixing. These two processes promote overturning and a more efficient replenishment of nutrients in the surface layers of the ocean.

[30] The annually averaged differences aim to show if summer or winter processes dominate for each nutrient. The difference in surface [P] (Figure 5, top) corresponds to a decrease by up to 0.02 $\mu$M in the Southern Ocean showing that the summer effect is greater than the winter. In fact in the Northern Hemisphere the two processes seem to cancel each other. South of ~55°S, the difference in surface [Si] (Figure 5, middle left) corresponds to an increase by up to 0.2 $\mu$M in the Southern Ocean showing that the winter effect is greater than the summer effect whereas north of ~55°S the annual average of difference corresponds to an increase in surface [Si] showing that the summer effect dominates in that zone. However in the Northern Hemisphere the two processes roughly cancel each other. The difference in surface iron ([Fe]) (Figure 5, bottom) corresponds to an increase by up to 0.03 nM in the Southern Ocean showing that the winter effect is larger than the summer effect.

[31] The asymmetry of the response between the Northern Hemisphere and the Southern Hemisphere is probably due to the winter response of SIC and vertical mixing which is stronger in the Southern Hemisphere than in the Northern Hemisphere [*Manizza et al.*, 2005].

### 3.4. Phytoplankton Dynamics

[32] Phytoplankton dynamics are mainly controlled by nutrient and light availability and by zooplankton grazing activity. Nutrient and light availability are directly con-

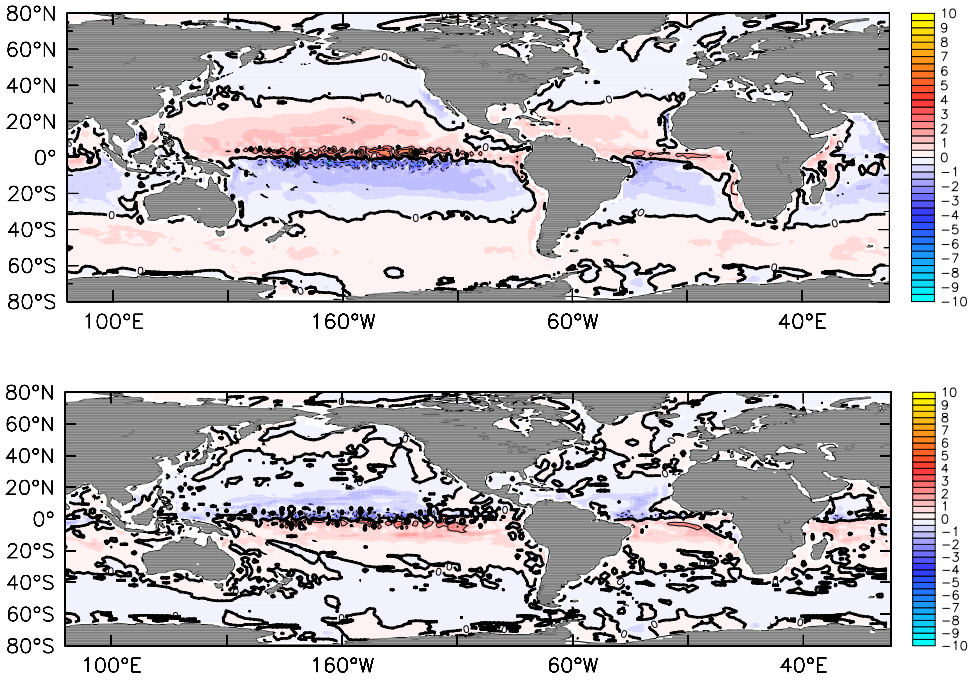


**Figure 3.** Annual average of difference (Green Ocean minus Blue Ocean) in the meridional component of velocity at (top) surface and (bottom) 50 m depth. Positive values indicate poleward currents and units are $10^{-2}$ m $s^{-1}$.

trolled by upper ocean physical properties (stratification, circulation, and SIC).

[33] Phytoplankton functional types have different affinities for light and nutrients (Table 1). To quantify the contribution of each PFT to the total phytoplankton biomass of the pelagic ecosystem, we define the relative contribution to chlorophyll (RCC) in percent for each PFT as

$$RCC = \frac{[Chl]_{PFT}}{[Chl]_{TOTAL}} \cdot 100. \quad (7)$$

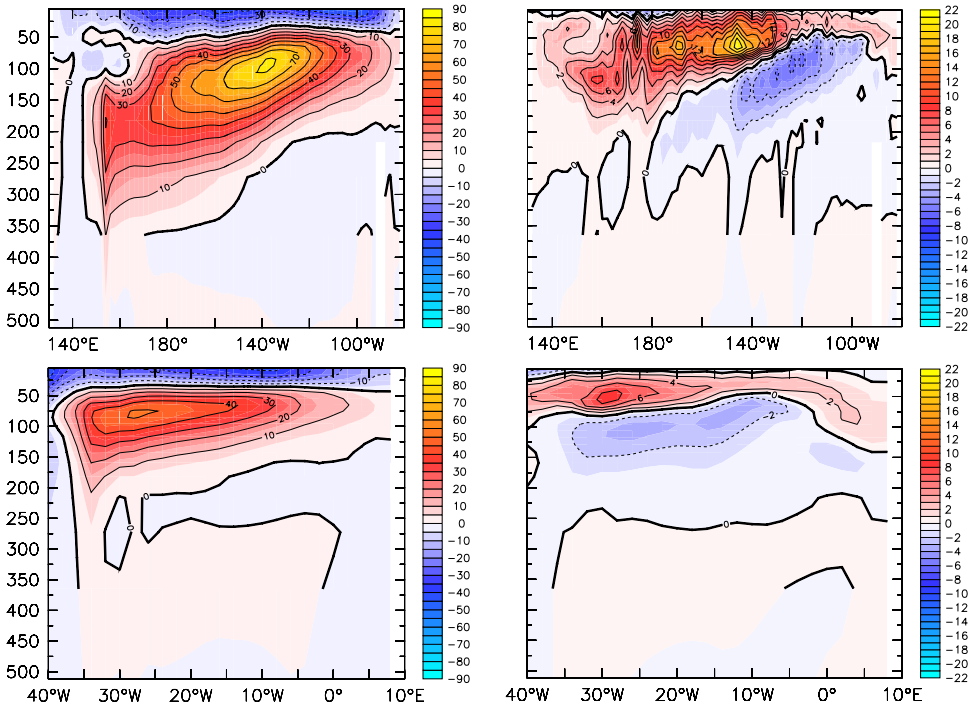


**Figure 4.** Annual average of zonal component of velocity at the equator in the (top left) Pacific Ocean and (bottom left) Atlantic Ocean and their difference (Green Ocean minus Blue Ocean) in the (top right) Pacific Ocean and (bottom right) Atlantic Ocean. Positive values indicate eastward currents, and units are $10^{-2}$ m $s^{-1}$.

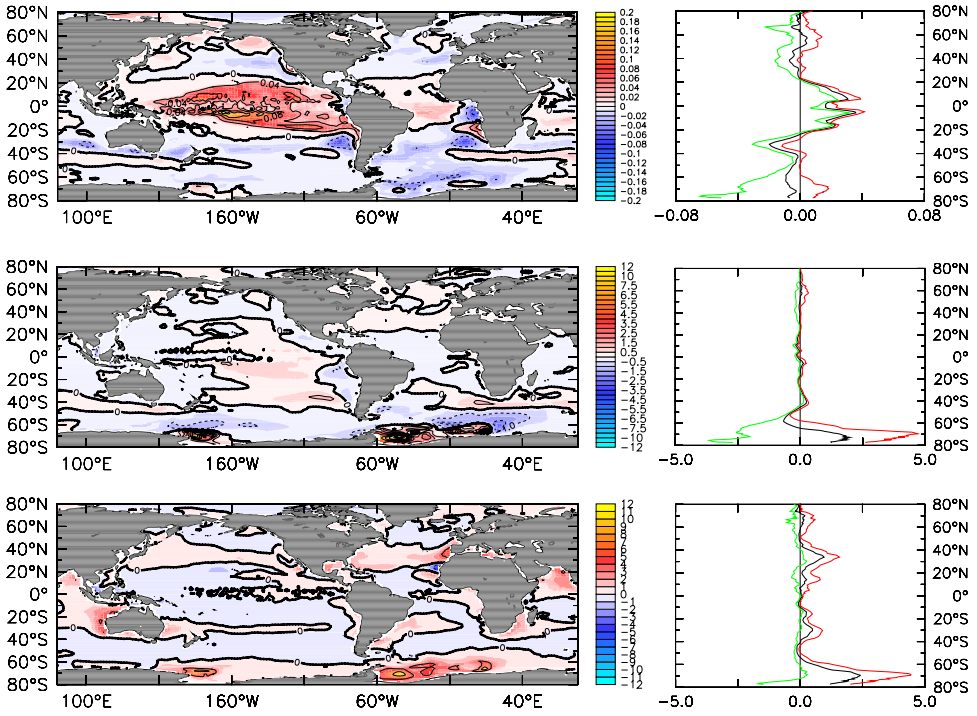


**Figure 5.** Annual average of differences (Green Ocean minus Blue Ocean) in surface (top left) P, (middle left) Si, and (bottom left) Fe concentrations. (right) Zonal difference for each nutrient with (black) annual, (red) maximum, and (green) minimum difference. Units are in $\mu$M for P and Si concentrations, and in $10^{-2}$ nM for Fe concentration.

The biologically induced physical modifications of the upper ocean favor some functional types and disfavor others. Below we report and comment on the surface values of RCC because they are the most representative of the changes caused by the light and nutrient modifications.

[34] We identify four main zones of the global surface ocean where major changes in pelagic ecosystem composition are found: (1) the tropical zones (between 10°N and 10°S), (2) the tropics/subtropics boundary zones (between 10° and 20° of both hemispheres) of the Pacific and Atlantic oceans, (3) the zones between 20° and 40° of both hemispheres, and (4) the Southern Ocean south of ~50°S. In the tropical oceans, the RCC of silicifiers increases by up to 1% at the expense of the other two PFTs (Figure 6). These relatively small changes are probably caused by a competitive advantage of silicifiers due to the increase in both [P] and [Fe] induced by the modifications in circulation of that area.

[35] In the tropics/subtropics boundary zones, the mixed phytoplankton RCC increases by up to 25% balanced by a decrease in calcifiers RCC due to the increase in phosphorus supply from the tropical zones (Figure 6). Mixed phytoplankton have a higher half-saturation constant ($K_P$) for phosphate. Since calcifiers are closer to the saturated part of the growth curve, the mixed phytoplankton benefit more from the additional nutrient supply and outcompete calcifiers. In the zones between 20° and 40° of both hemispheres, the RCC of calcifiers increases by up to 10% and this increase is balanced by a decrease in mixed phytoplankton RCC. This ecological shift can be explained by the decrease in surface nutrient concentration driven by the increase in stratification because calcifiers are better adapted to low nutrient concentration than mixed phytoplankton.

[36] In the Southern Ocean south of ~50°S, the RCC of silicifiers shows a substantial increase, by up to 18% partly balanced by a decrease in RCC of both mixed phytoplankton and calcifiers (Figure 6). In this region of the Southern Ocean, two main factors normally limit the growth of silicifiers: (1) light [*Mitchell et al.*, 1991] and (2) iron availability [*Martin*, 1990]. The PLF in our OBGCM reduces these limiting factors acting in different seasons, increasing stratification (and reducing light limitation) in summer and enhancing vertical mixing in winter with a more efficient replenishment of nutrients in the top layers of the ocean. The amplification of the seasonal cycle of MLD [*Manizza et al.*, 2005], due to the PLF, causes a reduction in light limitation in summer and an enhanced vertical nutrient supply in winter, as explained above, representing together an enhancing factor for the growth of silicifiers. The PLF has both positive and negative effects on the total biomass of phytoplankton at the ocean surface (Figure 6, top left) ($[Chl]_{surf}$ in mg $m^{-3}$).

[37] The PLF has positive effects on surface phytoplankton biomass both at high latitudes (because of alleviated light limitation) and in the areas of subtropical gyres closer to the tropics (because of alleviated nutrient limitation). However, in the zones between 20° and 40° of both hemispheres the PLF causes a decrease in $[Chl]_{surf}$ due to increase in stratification [*Manizza et al.*, 2005] which decreases the vertical nutrient supply.

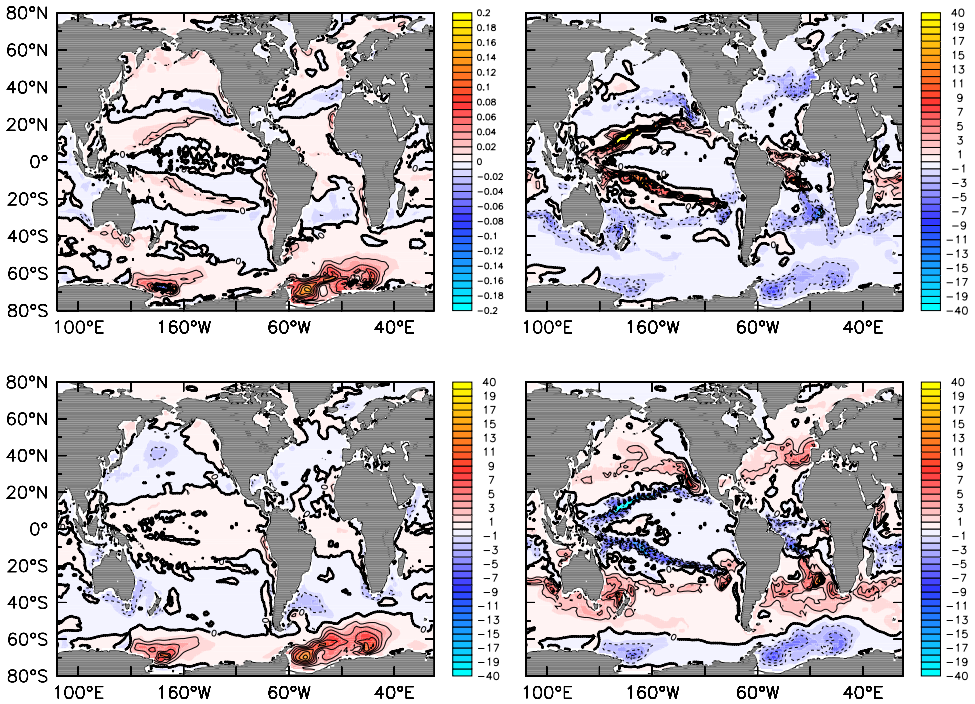


**Figure 6.** Annual average of difference (Green Ocean minus Blue Ocean) in (top left) surface [Chl] and surface relative contribution to total [Chl] of (top right) mixed phytoplankton, (bottom left) silicifiers, and (bottom right) calcifiers. Units are in mg $m^{-3}$ for surface [Chl] and percent for RCC of every PFT.

### 3.5. Primary Production

[38] In the tropical Atlantic and Pacific Oceans (roughly between 10°N and 10°S), total primary production (TPP), when integrated down the water column, shows a small decrease (∼5 gC $m^{-2}$ $a^{-1}$) (Figure 7, top left). The upward displacement of the EUC (Figure 4, right) caused by the PLF (mostly because of the MLD shoaling) causes an increase of nutrient supply (mostly phosphorus) in the upper part of the water column enhancing the productivity of those zones and, at the same time, it reduces the nutrient supply of the layers underneath causing a reduction in their productivity. When vertically integrated these two effects result in a net decrease of primary production of those zones meaning that the effect of reduction overcomes the effect of enhancement in that region.

[39] The lower zones of subtropical gyres of the Atlantic and Pacific oceans show a larger increase in surface primary production (∼4 gC $m^{-3}$ $a^{-1}$, not shown here). In those zones the vertically integrated TPP shows an increase by up to 40 gC $m^{-2}$ $a^{-1}$ (Figure 7, top left). In those regions, MLD shoals due to the PLF (Figure 2, middle) and the phytoplankton productivity is mainly limited by scarce vertical nutrient supply caused by high degree of water column stratification. Considering that the PLF also enhances both the meridional advection from tropics to the subtropics and the vertical supply of phosphate in the tropics, we infer that only the increased lateral nutrient supply from the tropics to the subtropics could explain this increase in TPP. However in the upper rims of the subtropical gyres (at both ∼30°N and ∼30°S) TPP decreases because of the increase in stratification preventing vertical nutrient supply.

[40] At northern high latitudes, the increase in TPP by up to 4 gC $m^{-2}$ $a^{-1}$ (5%) (Figure 7, top left) is mainly due to calcifiers at the expense of mixed phytoplankton favored by the increase in stratification. In the Southern Ocean, the TPP increases by up to 15 gC $m^{-2}$ $a^{-1}$ (35%) mainly driven by the relative increase in TPP of calcifiers (north of ∼50°S) and by silicifiers (south of ∼50°S).

[41] Globally, in the Blue Ocean version of PlankTOM5, TPP is 71 PgC $a^{-1}$ and because of the PLF the TPP increases by 650 TgC $a^{-1}$ (∼1%) (Table 2). This increase is mostly due to the increase occurring in the subtropical regions (in the Northern Hemisphere and in the Southern Hemisphere by 410 and 210 TgC $a^{-1}$, respectively) where TPP is boosted by the increased nutrient supply.

### 3.6. Pelagic Biogenic Calcification

[42] In the OBGCM the process of pelagic biogenic calcification (PBC) is carried out by calcifiers. The modifications of vertically integrated values of PBC partly follow the geographical patterns of change in RCC of calcifiers. PBC (Figure 7, bottom left) shows a substantial increase in the subtropical gyres by up to 20 gC-$CaCO_3$ $m^{-2}$ $a^{-1}$ (25%) with a maximum in the Pacific Ocean, and a smaller increase at high latitudes of both hemispheres by up to 5 gC-$CaCO_3$ $m^{-2}$ $a^{-1}$ (5%). In fact in the Southern Ocean, the latitude of ∼55°S represents a clear divide for the change in PBC. North of 55°S the PBC increases owing to the relative increase in calcifiers RCC because of the increase in stratification. South of 55°S the PBC decreases owing to the relative increase in silicifiers RCC caused by the increase in iron supply. Globally, in the Blue Ocean version of PlankTOM5, PBC is 23 PgC $a^{-1}$ and it shows a

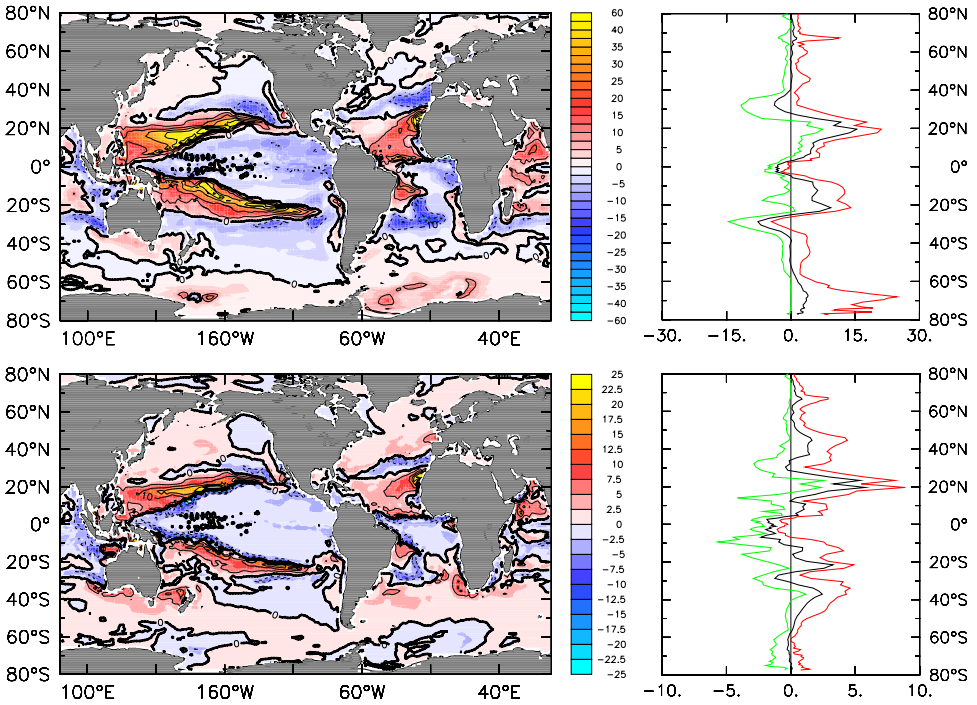


**Figure 7.** Vertically integrated differences (Green Ocean minus Blue Ocean) in (top) total primary production and (bottom) pelagic biogenic calcification. (left) Global distribution of annual average of difference. (right) Zonal values of (black) annual, (red) maximum, and (green) minimum difference. Units are gC $m^{-2}$ $a^{-1}$ for primary production and gC-$CaCO_3$ $m^{-2}$ $a^{-1}$ for pelagic biogenic calcification.

relative increase by 207 TgC-$CaCO_3$ $a^{-1}$ (∼1%) (Table 2). The PBC increases everywhere except in the tropical zones (−56 TgC-$CaCO_3$ $a^{-1}$) where the increase of supply of phosphate favors mixed phytoplankton at the expenses of calcifiers (Table 2). The zones showing the greatest increase in PBC are the northern subtropics (115 TgC-$CaCO_3$ $a^{-1}$) due to increased nutrient supply and the southern high latitudes (75 TgC-$CaCO_3$ $a^{-1}$) due to the mechanisms previously explained.

### 3.7. POC and $CaCO_3$ Export Production

[43] In PlankTOM5 the export of particulate organic carbon (EP) is not only driven by primary production but also by ecosystem composition. Globally, in the Blue Ocean version of PlankTOM5, EP is 5 PgC $a^{-1}$ and the PLF cause a global decrease by 257 TgC $a^{-1}$ (∼6%). The PLF causes a general decrease in EP over the global ocean by up to 2 gC $m^{-2}$ $a^{-1}$, except in the Southern Ocean south of 50°S (Figure 8, top) and in the subtropical zones where TPP has shown an increase. The change in EP is mainly driven by the shift in relative abundance of calcifiers that increase their RCB at the expense of silicifiers as shown above. The ecosystem shift translates in a greater production of smaller compared to bigger particles with a consequent decrease in EP.

[44] However in the far south of the Southern Ocean, the increase in EP by up to 4 gC $m^{-2}$ $a^{-1}$ is due to the increase in RCB of silicifiers. Silicifiers favor the production of big POC particles which drive a more efficient export of organic carbon. The EP shows a relative global decrease by 650 TgC $a^{-1}$ with all the zonally averaged regions of the global ocean except the Southern Ocean (south of 50°S) showing

**Table 2.** Summary of Modifications of Both Air-Sea Fluxes (Oxygen and Carbon Dioxide) and of the Key Diagnostics Associated With the Ocean Carbon Cycle[a]

| Regions | $\Delta O_2$ Flux (Tmol$O_2$ $a^{-1}$) | $\Delta CO_2$ Flux (TgC $a^{-1}$) | ΔTPP (TgC $a^{-1}$) | ΔPBC (TgC-$CaCO_3$ $a^{-1}$) | ΔPOC-EP (TgC $a^{-1}$) | $\Delta CaCO_3$-EP (TgC-$CaCO_3$ $a^{-1}$) |
|---|---|---|---|---|---|---|
| North of 30°N | −5 | 22 | −30 (−0.3) | 33 (1.3) | −28 (−3.4) | 5 (1.2) |
| 10°N–30°N | 1 | −8 | 410 (3.6) | 115 (2.6) | −33 (−4.3) | 16 (2) |
| 10°N–10°S | −13 | 85 | 70 (0.3) | −56 (−0.8) | −110 (−8.1) | −12 (−1) |
| 10°S–30°S | −6 | −8 | 210 (1.5) | 33 (0.7) | −68 (−3.9) | 5 (0.6) |
| South of 30°S | −23 | −19 | −10 (−0.01) | 75 (2) | −36 (−2.8) | 12 (1.9) |
| Global | −46 | 72 | 650 (1) | 207 (1) | −275 (−5.5) | 27 (0.7) |

[a]Annual average of differences are both zonally and meridionally integrated over the zones shown in the table. Differences refer to Green Ocean minus Blue Ocean. Positive values of air-sea fluxes anomalies correspond to relative outgassing. The prefix T corresponds to Tera ($10^{12}$). Values in brackets correspond to the incremental change respect to the values in the Blue Ocean run; units are percent.

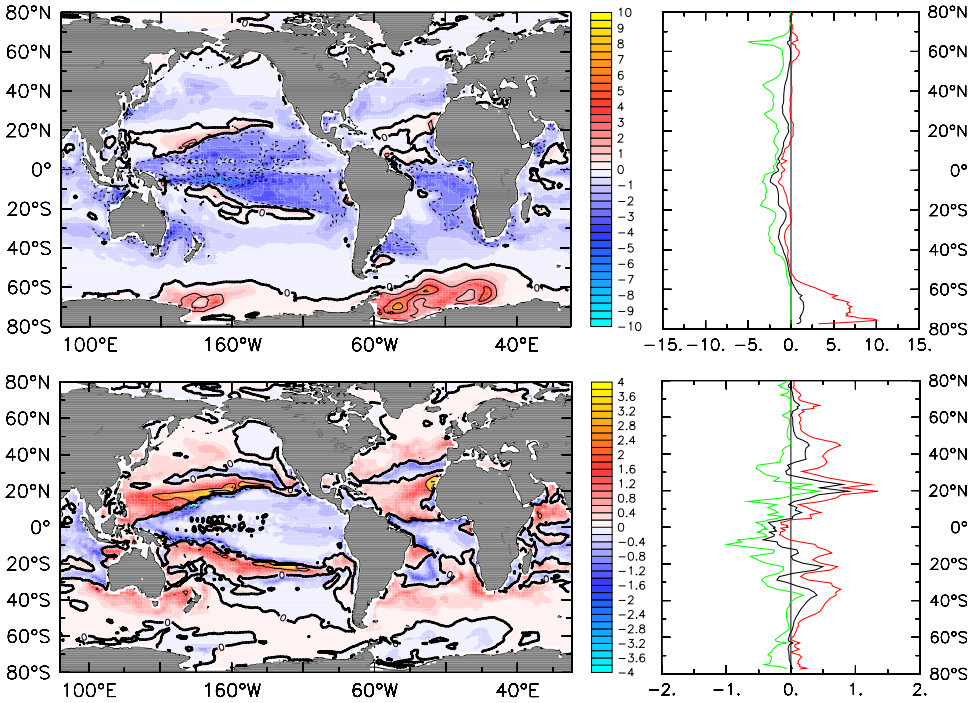


**Figure 8.** Differences (Green Ocean minus Blue Ocean) in export production of both (top) POC and (bottom) $CaCO_3$. (left) Global distribution of annual average of difference. (right) Zonal values of (black) annual, (red) maximum, and (green) minimum difference. Units are gC $m^{-2}$ $a^{-1}$ for POC export and gC-$CaCO_3$ $m^{-2}$ $a^{-1}$ for $CaCO_3$ export.

the same pattern. Globally, in the Blue Ocean version of PlankTOM5, EC is 4 PgC $a^{-1}$ and it shows an increase by 27 TgC-$CaCO_3$ $a^{-1}$ (∼1%) (Table 2) because of the PLF. The differences in Export Production of $CaCO_3$ (EC) follow the same geographical patterns as the PBC differences (Figure 8, bottom panels), with an increase in EC in the lower part of the subtropical gyres of both hemispheres by up to ∼4 gC-$CaCO_3$ $m^{-2}$ $a^{-1}$ (∼40%).

### 3.8. $CO_2$ and $O_2$ Air-Sea Fluxes

[45] The PLF modifies the physical structure of the upper ocean and indirectly impacts the biogeochemical processes with consequences for air-sea fluxes of $CO_2$ and $O_2$. We present in this section differences of air-sea fluxes caused by the PLF, which we discuss by zones from the tropics to high latitudes.

[46] In the tropical Pacific and Atlantic oceans, the PLF produces a relative outgassing of $CO_2$ by up to 0.6 molC $m^{-2}$ $a^{-1}$ (Figure 9, top left) and a relative ingassing of $O_2$ by up to 0.5 mol$O_2$ $m^{-2}$ $a^{-1}$ (Figure 9, bottom left). The decrease in EP and TPP, caused by the PLF, are the main drivers for the relative outgassing of $CO_2$ and relative ingassing $O_2$, respectively, in the tropical Pacific and Atlantic oceans.

[47] In the subtropical zones of the Atlantic and Pacific oceans air-sea fluxes show a relative ingassing of $CO_2$ (by up to 0.5 molC $m^{-2}$ $a^{-1}$) and a relative outgassing of $O_2$ (by up to 2.7 mol$O_2$ $m^{-2}$ $a^{-1}$). These are driven by the increase in EP and the TPP, respectively.

[48] At high latitudes of both hemispheres, both a SST warming in spring/summer and a more vigorous mixing in autumn/winter cause a relative outgassing of $CO_2$ by up to 0.2 molC $m^{-2}$ $a^{-1}$ (Figure 10, top left). In the same zones, the $O_2$ fluxes exhibit a relative ingassing by up to 0.5 mol$O_2$ $m^{-2}$ $a^{-1}$ showing that the mixing effect in fall/winter exceeds the warming effect in spring/summer. In the Southern Ocean, the PLF causes a relative $CO_2$ outgassing (by up to 2.5 molC $m^{-2}$ $a^{-1}$) and a relative $O_2$ ingassing (12 mol$O_2$ $m^{-2}$ $a^{-1}$) mainly due to the reduction in SIC which promotes vertical mixing and consequent modification of air-sea fluxes.

[49] The PLF also amplifies the seasonal cycle of air-sea fluxes of $CO_2$ and $O_2$ in the extratropical zones poleward of 10° of both hemispheres (Figure 10, top). The main driver of this amplification is the amplification of the seasonal cycle of ocean physical properties, mainly SST (Figure 2, top) as also shown in other studies [*Shell et al.*, 2003; *Manizza et al.*, 2005], that consequently drive the amplification of the seasonal cycle of biogeochemical processes such as TPP and PBC. In spring/summer the SST warming caused by the biophysical feedback mostly drives the outgassing of $CO_2$ and $O_2$ (Figure 9, right) to which are summed the effect of enhanced PBC and TPP, respectively. In fall/winter the enhanced $CO_2$ and $O_2$ ingassing is mostly driven by the SST cooling (Figure 2, top) except in some regions of the Southern Ocean south of ∼50°S. On global scale the flux of $O_2$ shows an anomaly of ingassing (46 Tmol$O_2$ $a^{-1}$) (Table 2). Such anomaly can be comparable with interannual variability of $O_2$ oceanic flux as estimated by *Rödenbeck et al.* [2008]. We identify that there are two key regions driving the flux into the ocean: (1) the southern high latitudes (23 Tmol$O_2$ $a^{-1}$) and (2) the tropical regions (13 Tmol$O_2$ $a^{-1}$). The reduction in SIC (and its impact on vertical mixing) in the southern high

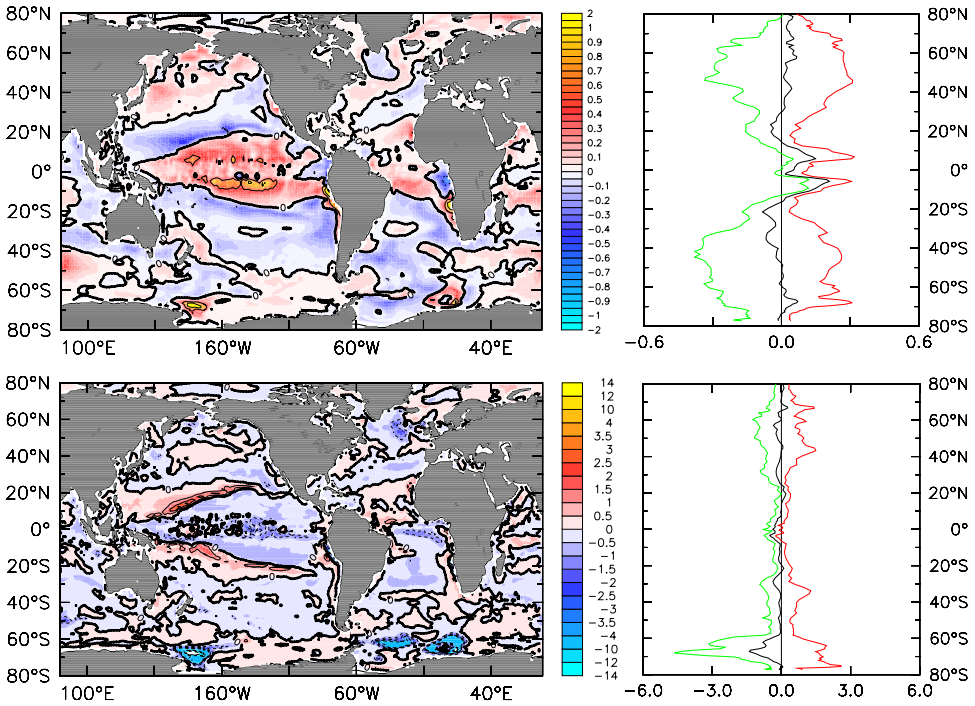


**Figure 9.** Difference (Green Ocean minus Blue Ocean) in (top) $CO_2$ and (bottom) $O_2$ air-sea fluxes. (left) Global maps of annual average of difference and (right) zonal values of (black) average, (red) maximum, and (green) minimum difference in air-sea fluxes. Positive values indicate outgassing and units are mol $m^{-2}$ $a^{-1}$.

latitudes and the decrease in TPP in the tropical zones are the main processes driving the change of the $O_2$ air-sea fluxes. A comparison of the changes in fluxes in the tropics (13 $TmolO_2$ $a^{-1}$) and in the extratropics (33 $TmolO_2$ $a^{-1}$) reveals that the extratropics dominate the change in global fluxes of $O_2$. However considering the global perturbation in $CO_2$ air-sea flux, the tropics (85 TgC $a^{-1}$) drive the outgassing anomaly. Considering the global $CO_2$ and $O_2$

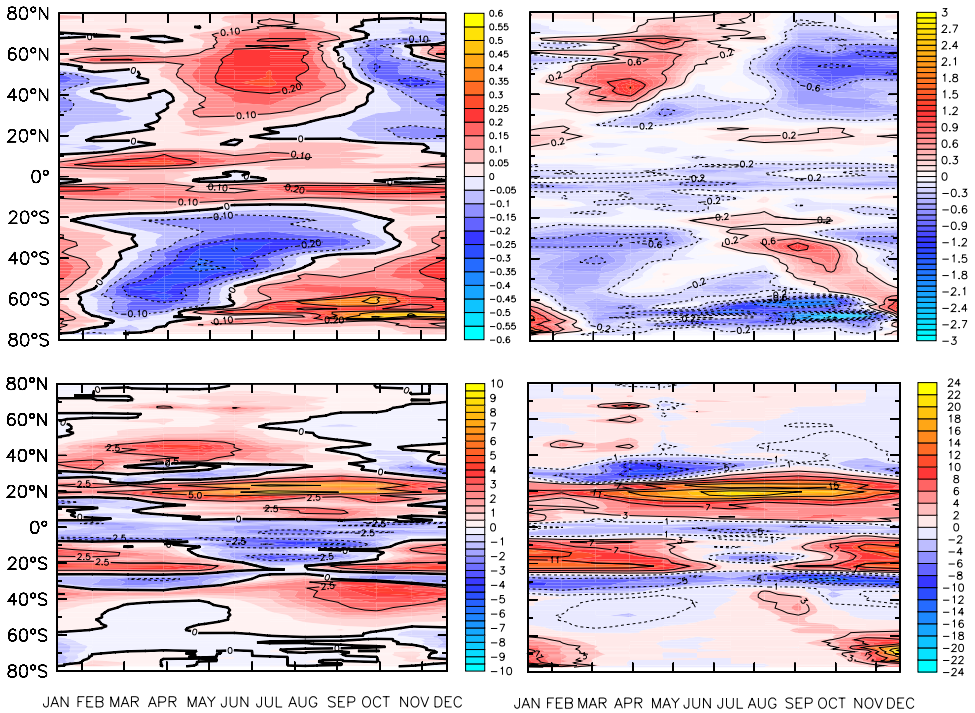


**Figure 10.** Time/latitude plot of difference in air-sea fluxes of (top left) $CO_2$ and (top right) $O_2$ and vertically integrated (bottom left) PBC and (bottom right) TPP. Units are mol $m^{-2}$ $a^{-1}$ for air-sea fluxes, gC-$CaCO_3$ $m^{-2}$ $a^{-1}$ for PBC, and gC $m^{-2}$ $a^{-1}$ for TPP.

flux anomalies, the perturbation caused by the PLF is not remarkable although both physical and biogeochemical processes are impacted by the PLF at the same time with consequences for air-sea gas exchange. We propose two main arguments to explain the results from this modeling study. First, we have shown that for each region of the global ocean several processes are impacted by the PLF and in some cases they tend to reenforce each other (the relative $O_2$ outgassing in the high latitude oceans in the warming season due to both SST warming and TPP increase) but in other cases they tend to oppose each other such as the change in $CO_2$ flux at northern high latitudes where in the warming season the increase in SST and the increase in PBC tend to counteract each other. Second, with the division of the global ocean in five regions we have shown that for a given gas the net effect is different from region to region so then when integrated over the global domain the impact of the PLF is not substantial.

## 4. Discussion and Conclusions

[50] In this study we have explicitly represented the PLF in a global OBGCM to explore the biophysical impact on biogeochemical processes. We have highlighted that the changes in ocean physical processes have several impacts on ocean biogeochemical processes with consequences for the air-sea fluxes of soluble gases. We have shown that, especially at high latitudes, the inclusion of the PLF results in an amplification of the seasonal cycle of air-sea gas exchange mostly driven by the SST amplification plus that of TPP (for $O_2$) and PBC (for $CO_2$). However on a global scale the impact of this feedback is rather small because the multiple feedbacks in several cases tend to oppose each other. Our results are consistent with other studies in the extratropical zones [*Murtugudde et al.*, 2002; *Oschlies*, 2004; *Wetzel et al.*, 2006] while in the tropical zones are in agreement only with some of those. This feature strongly depends on the fact that the bio-optical parameterizations implemented vary from study to study both in the control run (comparable to our Blue Ocean) and in the perturbation run (comparable to our Green Ocean run). Therefore we think that the biogeochemical response and also the associated response of air-sea fluxes can be considered robust in the extratropics and more model dependent in the tropics.

[51] The classical view of the processes regulating the exchange of $CO_2$ and $O_2$ between the ocean and atmosphere is that two main processes are involved: first, the solubility pump and second, the biological pump. The physical properties are the main factors directly impacting the efficiency of the solubility pump [*Ito and Follows*, 2003; *Toggweiler et al.*, 2003a]. The biological process such as TPP acts directly to modulate the efficiency of the biological pump (or "soft tissue") [*Murnane et al.*, 1999; *Toggweiler et al.*, 2003b]. Moreover, the physical properties of the ocean can indirectly impact the efficiency of the biological pump by modulating the nutrients and light availability in the upper ocean. This study reveals that the biophysical feedback modifies ocean physical properties and thus controls the efficiency of the solubility pump. By using an OBGCM we have explored the biogeochemical feedbacks on air-sea fluxes of $CO_2$ and $O_2$. This study has demonstrated that the PLF can be considered as a new potential missing link between the solubility and the biological pump in the ocean.

[52] This study has revealed that the inclusion of the PLF in an OBGCM impacts the physical properties of the tropical oceans with consequences for the lateral advection of nutrients to the subtropical zones of both hemispheres in the Pacific and Atlantic basins. *Williams et al.* [2006] have shown that the advection of nutrients from the tropics to the subtropics is an essential process to sustain biological productivity in the oligotrophic subtropical North Atlantic. The combination of our study with the modeling work of *Williams et al.* [2006] would suggest that the bio-optical state of the tropical oceans can influence subtropical gyres productivity via ocean circulation and nutrient transport.

[53] Climate models forced by future scenarios of increasing atmospheric [$CO_2$] have shown substantial changes in oceanic physical properties. Changes such as SST warming, MLD shoaling [*Sarmiento et al.*, 1998; *Friedlingstein et al.*, 2001], reduction in both deep water formation [*Manabe and Stouffer*, 1993] and SIC [*Flato*, 2004] could potentially impact the present geographical distribution of phytoplankton biomass and their abundance as shown by several studies [*Bopp et al.*, 2001; *Pierce*, 2004; *Sarmiento et al.*, 2004].

[54] Changes in the distribution of phytoplankton biomass might in turn modify the functioning of the PLF evaluated in this study for present climate conditions. Its modification by climate change might potentially trigger further physical and biogeochemical feedbacks in the ocean.

[55] **Acknowledgments.** We thank the OPA team and K. Rodgers for their assistance in the model simulations and for providing the forcing data. This paper greatly benefited form the discussions with the participants of the Dynamic Green Ocean Project, in particular Shuba Sathyendranath and Trevor Platt. MM is grateful to Anand Gnanadesikan and Raffele Ferrari for enlightening discussions on ocean dynamics. We also thank the German Center for Climate Research (DKRZ) in Hamburg for computer time. Ferret from NOAA/PMEL has been used to make the plots. ETB and MM were supported both by the Northern Ocean Carbon Exchange Process EU-Project (contract EVK2-CT-2001-00134) and CARBOOCEAN.

## References

Aumont, O., E. Maier-Reimer, S. Blain, and P. Monfray (2003), An ecosystem model of the global ocean including Fe, Si, P colimitations, *Global Biogeochem. Cycles*, *17*(2), 1060, doi:10.1029/2001GB001745.

Ballé, J. (1998), Simulation des champs de chlorophylle de surface et flux océan-atmosphère de $CO_2$ durant les années FOCAL (1982–1984) dans l'Atlantique, Ph.D. thesis, Univ. Pierre et Marie Cure, Paris.

Bopp, L. (2001), Changements climatiques et biogéochemie marine: Modélisation du dernier maximum glaciaire et de l'Ére industrielle, Ph.D. thesis, Univ. Pierre et Marie Cure, Paris.

Bopp, L., P. Monfray, O. Aumont, J. L. Dufresne, H. L. Treut, G. Madec, L. Terray, and J. C. Orr (2001), Potential impact of climate change on marine export production, *Global Biogeochem. Cycles*, *15*(1), 81–99.

Bopp, L., K. E. Kohfeld, C. Le Quéré, and O. Aumont (2003), Dust impact on marine biota and atmospheric $CO_2$ during glacial periods, *Paleoceanography*, *18*(2), 1046, doi:10.1029/2002PA000810.

Conkright, M. E., H. E. Garcia, T. D. O'Brien, R. A. Locarnini, T. P. Boyer, C. Stephens, and J. I. Antonov (2002), *World Ocean Atlas*, vol. 4, *Nutrients, NOAA Atlas NESDIS*, vol. 52, NOAA, Silver Spring, Md.

Fichefet, T., and M. A. Morales-Maqueda (1999), Modelling the influence of snow accumulation and snow-ice formation on the seasonal cycle of the Antarctic sea-ice cover, *Clim. Dyn.*, *15*, 251–268.

Flato, G. M. (2004), Sea-ice and its response to $CO_2$ forcing as simulated by global ocean climate models, *Clim. Dyn.*, *23*, 229–241.

Foujols, M., M. Lévy, O. Aumont, and G. Madec (2000), *OPA8.1 Tracer Model Reference Manual*, Inst. Pierre Simon Laplace, Paris.

Friedlingstein, P., L. Bopp, P. Ciais, J. L. Dufresne, L. Fairhead, H. L. Treut, P. Monfray, and J. Orr (2001), Positive feedback between future climate change and the carbon cycle, *Geophys. Res. Lett.*, *28*(8), 1543–1546.

Gaspar, P., Y. Gregoris, and J. M. Lefèvre (1990), A simple kinetic energy model for simulations of the oceanic vertical mixing: Tests at station Papa and Long-Term Upper Ocean Study Site, *J. Geophys. Res.*, *95*(C9), 16,179–16,193.

Gent, P. R., and J. C. McWilliams (1990), Isopycnal mixing in the ocean circulation models, *J. Phys. Oceanogr.*, *20*, 150–155.

Goosse, H. (1997), Modelling the large-scale beahviour of the coupled sea-ice system, Ph.D. thesis, Univ. Catholique de Louvain, Louvain, Belgium.

Ito, T., and M. J. Follows (2003), Upper ocean control on the solubility pump of $CO_2$, *J. Mar. Res.*, (61), 465–489.

Kahru, M., J.-M. Leppanen, and O. Rud (1993), Cyanobacterial blooms cause heating of the sea-surface, *Mar. Ecol. Prog. Ser.*, *101*, 1–7.

Kalnay, E., et al. (1996), The NCEP/NCAR 40-year reanalysis project, *Bull. Am. Meteorol. Soc*, *77*, 437–471.

Kara, A. B., H. E. Hurlburt, P. A. Rochford, and J. J. O'Brien (2004), The impact of water turbidity on interannual sea surface temperature simulations in a layered global ocean model, *J. Phys. Oceanogr.*, *34*, 345–359.

Key, R. M., A. Kozyr, C. L. Sabine, K. Lee, R. Wanninkhof, J. L. Bullister, R. A. Feely, F. J. Millero, C. Mordy, and T.-H. Peng (2004), A global ocean carbon climatology: Results from Global Data Analysis Project (GLODAP), *Global Biogeochem. Cycles*, *18*, GB4031, doi:10.1029/2004GB002247.

Le Quéré, C., et al. (2005), Ecosystem dynamics based on plankton functional types for global ocean biogeochemistry models, *Global Change Biol.*, *11*, 2016–2040, doi:10.1111/j.1365-2486.2005.01004.x.

Levitus, S. (1982), Climatological atals of the world ocean, *Prof. Pap. 13*, 173 pp., NOAA, Silver Spring, Md.

Levitus, S., and T. P. Boyer (1994), *World Ocean Atlas*, vol. 2, *Oxygen*, *NOAA Atlas NESDIS*, vol. 2, 220 pp., NOAA, Silver Spring, Md.

Madec, G., and M. Imbard (1996), A global ocean mesh to overcome the north pole singularity, *Clim. Dyn.*, *12*, 381–388.

Madec, G., P. Delecluse, M. Imbard, and C. Lévy (1999), *OPA 8.1 Ocean General Circulation Model Reference Manual*, Lab. d'Océanogr. Dyn. et de Climatol., Paris.

Manabe, S., and R. J. Stouffer (1993), Century-scale effects of increased atmospheric $CO_2$ on the ocean-atmosphere system, *Nature*, *364*, 215–218.

Manizza, M. (2006), Modelling phytoplankton-light feedback and its biogeochemical implications, Ph.D. thesis, School of Environ. Sci., Univ. of E. Anglia, Norwich, UK.

Manizza, M., C. Le Quéré, A. J. Watson, and E. T. Buitenhuis (2005), Bio-optical feedbacks among phytoplankton, upper ocean physics and sea-ice in a global model, *Geophys. Res. Lett.*, *32*, L05603, doi:10.1029/2004GL020778.

Martin, J. H. (1990), Glacial-interglacial $CO_2$ changes: The iron hypothesis, *Paleoceanography*, *5*(1), 1–13.

Marzeion, B., A. Timmermann, R. Mutugudde, and F.-F. Jin (2005), Biophysical feedbacks in the tropical Pacific, *J. Clim.*, *18*, 58–70.

Mitchell, B. G., E. A. Brody, O. Holm-Hansen, C. McClain, and J. Bishop (1991), Light limitation oh phytoplankton biomass and macronutrients utilization in the Southern Ocean, *Limnol. Oceanogr.*, *36*(8), 1662–1677.

Morel, A. (1988), Optical modelling of the upper ocean in relation to its biogenous matter content (case I waters), *J. Geophys. Res.*, *93*(C9), 10,749–10,768.

Murnane, R., J. L. Sarmiento, and C. Le Quéré (1999), Spatial distribution of air-sea $CO_2$ fluxes and the interhemispheric transport of carbon by the oceans, *Global Biogeochem. Cycles*, *13*(2), 287–305.

Murtugudde, R., J. Beauchamp, C. R. McClain, M. Lewis, and A. J. Busalacchi (2002), Effects of penetrative radiation on the upper tropical ocean circulation, *J. Clim.*, *15*, 470–486.

Nakamoto, S., S. P. Kumar, J. M. Oberhuber, K. Muneyama, and R. Frouin (2000), Chlorophyll modulation of sea surface temperature in the Arabian Sea in a mixed-layer isopycnal general circulation model, *Geophys. Res. Lett.*, *27*(6), 747–750.

Nakamoto, S., S. P. Kumar, J. M. Oberhuber, J. Ishizaka, K. Muneyama, and R. Frouin (2001), Response of the equatorial Pacific to chlorophyll pigment in a mixed layer isopycnal ocean general circulation model, *Geophys. Res. Lett.*, *28*(1), 2021–2024.

Oschlies, A. (2004), Feedbacks of biotically induced radiative heating on upper-ocean heat budget, circulation, and biological production in a coupled ecosystem-circulation model, *J. Geophys. Res.*, *109*, C12031, doi:10.1029/2004JC002430.

Paulson, C. A., and J. J. Simpson (1977), Irradiance measurements in the upper ocean, *J. Phys. Oceanogr.*, *7*, 952–956.

Pierce, D. W. (2004), Future changes in biological activity in the North Pacific due to anthropogenic forcing on the physical environment, *Clim. Change*, *62*, 389–418.

Rödenbeck, C., C. Le Quéré, R. F. Keeling, and M. Heimann (2008), Estimating interannual variability of oceanic biogeochemistry from atmospheric $O_2/N_2$ and $CO_2$ measurements, *Tellus, Ser. B*, in press.

Sarmiento, J. L., J. C. Orr, and U. Siegenthaler (1992), A perturbation simulation of $CO_2$ uptake in an ocean general circulation model, *J. Geophys. Res.*, *97*(C3), 3621–3645.

Sarmiento, J. L., T. M. C. Hughes, R. J. Stouffer, and S. Manabe (1998), Simulated response of the ocean carbon cycle to anthropogenic climate warming, *Nature*, *393*, 245–249.

Sarmiento, J. L., et al. (2004), Response of ocean ecosystems to climate warming, *Global Biogeochem. Cycles*, *18*, GB3003, doi:10.1029/2003GB002134.

Sathyendranath, S., A. D. Gouveia, A. R. Shetye, P. Ravindran, and T. Platt (1991), Biological control of surface temperature in the Arabian Sea, *Nature*, *349*, 54–56.

Shell, K. M., R. Frouin, S. Nakamoto, and R. C. J. Somerville (2003), Atmospheric response to solar radiation absorbed by phytoplankton, *J. Geophys. Res.*, *108*(D15), 4445, doi:10.1029/2003JD003440.

Sweeney, C., A. Gnanadesikan, S. M. Griffies, M. J. Harrison, A. Rosati, and B. Samuels (2005), Impacts of shortwave penetration depth on large-scale ocean circulation and heat transport, *J. Phys. Oceanogr.*, *35*, 1103–1119.

Timmermann, A., and F. F. Jin (2002), Phytoplankton influences on tropical climate, *Geophys. Res. Lett.*, *29*(23), 2104, doi:10.1029/2002GL015434.

Timmermann, R., H. Goosse, G. Madec, T. Fichefet, C. Ethe, and V. Duliere (2005), On the representation of high latitude processes in the ORCA-LIM global coupled seaice-ocean model, *Ocean Modell.*, (8), 175–201.

Toggweiler, J. R., A. Gnanadesikan, S. Carson, R. Murnane, and J. L. Sarmiento (2003a), Representation of the carbon cycle in box models and GCMs: 1. Solubility pump, *Global Biogeochem. Cycles*, *17*(1), 1026, doi:10.1029/2001GB001401.

Toggweiler, J. R., R. Murnane, S. Carson, A. Gnanadesikan, and J. L. Sarmiento (2003b), Representation of the carbon cycle in box models and GCMs: 2. Organic pump, *Global Biogeochem. Cycles*, *17*(1), 1027, doi:10.1029/2001GB001841.

Wanninkhof, R. (1992), Relationship between wind speed and gas exchange over the ocean, *J. Geophys. Res.*, *97*(C5), 7373–7382.

Weiss, R. F. (1970), The solubility of nitrogen, oxygen and argon in water and seawater, *Deep Sea Res.*, *17*, 712–735.

Wetzel, P., E. Maier-Reimer, M. B. amd, J. Jungclaus, N. Keenlyside, and M. Latif (2006), Effects of ocean biology on the penetrative radiation in a coupled climate model, *J. Clim.*, *19*, 3973–3987.

Williams, R. G., V. Roussenov, and M. J. Follows (2006), Nutrient streams and their induction into the mixed layer, *Global Biogeochem. Cycles*, *20*, GB1016, doi:10.1029/2005GB002586.

E. T. Buitenhuis, C. Le Quéré, and A. J. Watson, School of Environmental Sciences, University of East Anglia, Norwich NR4 7TJ, UK. (E.Buitenhuis@uea.ac.uk; C.Lequere@uea.ac.uk; A.J.Watson@uea.ac.uk)

M. Manizza, Program in Atmospheres, Oceans and Climate, Department of Earth, Atmospheric and Planetary Sciences, Massachusetts Institute of Technology, 77 Massachusetts Avenue, Cambridge, MA 02139, USA. (mmanizza@ocean.mit.edu)